Bulk permittivity, low frequency relaxation and the magnetic properties of $Pb(Fe_{1/2}Nb_{1/2})O_3$ ceramics

2010 J. Phys.: Condens. Matter 22 025901

(http://iopscience.iop.org/0953-8984/22/2/025901)

J. Phys.: Condens. Matter **22** (2010) 025901 (8pp) doi:10.1088/0953-8984/22/2/025901

Bulk permittivity, low frequency relaxation and the magnetic properties of $Pb(Fe_{1/2}Nb_{1/2})O_3$ ceramics

R K Mishra[1,4], R N P Choudhary[2] and A Banerjee[3]

[1] Department of Physics, V. N. Autonomous College, Jajpur Road, Jajpur 755019, Orissa, India
[2] Department of Physics and Meteorology, I.I.T., Kharagpur 721302, India
[3] UGC-DAE Consortium for Scientific Research, University Campus, Khandwa Road, Indore 452017, India

E-mail: rkm.phy@gmail.com

Received 22 May 2009, in final form 4 October 2009
Published 9 December 2009
Online at stacks.iop.org/JPhysCM/22/025901

Abstract

A $Pb(Fe_{1/2}Nb_{1/2})O_3$ ceramic sample was prepared through a high temperature solid-state reaction technique. The formation of a single-phase perovskite compound was confirmed by an x-ray diffraction technique. Dielectric and impedance parameters were measured as a function of frequency (10^2–10^6 Hz) at different temperatures (28–200 °C). The results were described using an equivalent circuit model and by extending the universal capacitor concept introduced by Jonscher. Bulk permittivity of the material and the power law exponent (extracted from impedance data) exhibits an anomaly at a particular temperature related to the ferroelectric–paraelectric transition. A slow relaxation process has been observed in the vicinity of the transition temperature. Temperature dependent magnetization (2–300 K) was measured at different magnetic fields in both zero-field-cooled (ZFC) and field-cooled (FC) modes. An antiferromagnetic transition was observed at 158 K but an unusual increase in magnetization below this transition indicates the onset of weak ferromagnetism at low temperature in this system. Nonlinear M–H and a finite opening in the hysteresis loop at 2 K substantiate the presence of ferromagnetic interactions. Significantly, a thermomagnetic history-dependent feature is observed below 9 K. The ZFC magnetization shows a sharp fall and it bifurcates from the monotonically increasing FC counterpart on decreasing temperature. This temperature, where ZFC magnetization shows a sharp peak, decreases with the increase in measurement field and it indicates the presence of a metastable magnetic state at low temperature.

1. Introduction

Lead iron niobate $Pb(Fe_{1/2}Nb_{1/2})O_3$ (PFN) belongs to the complex lead-based perovskite family of the general formula $Pb(B'_{1/2}B''_{1/2})O_3$, where B′ and B″ are lower and higher valence cations, respectively. Since the discovery of ferroelectricity in PFN in 1958 by Smolenskii *et al* [1], this material has been studied extensively because of its interesting dielectric properties [2–13] along with the existence of magnetic ordering [14–23]. The simultaneous occurrence of both ferroelectricity and magnetic ordering in the same phase is called the multiferroic property [24–27]. Recently multiferroic materials have received significant attention among researchers world wide due to the tremendous potential of these materials for industrial applications as well as the rich physics they involve [25–29]. In PFN, the multiferroic properties are achieved by sharing the B-site sublattice in the perovskite structure by both ferroelectrically active Nb^{5+} ions and magnetically active Fe^{3+} ions [2, 24, 25, 27]. The literature reveals that PFN shows a diffused ferroelectric transition like that of a relaxor but, unlike that of a relaxor, its transition temperature is independent of frequency [3, 4, 8, 30, 31]. This material has high dielectric loss due to the occurrence of Fe^{2+} ions and oxygen vacancies, which are detrimental to

[4] Author to whom any correspondence should be addressed.

its ferroelectric properties [22]. Its magnetic properties are also equally complex. It has been established that PFN shows G-type antiferromagnetic ordering below 140 K with weak ferromagnetism [15, 21, 24, 32]. However, there are different reports in the literature about the transition temperatures (ferroelectric and antiferromagnetic) and the number of magnetic transitions, which are sample-dependent [5, 22]. Due to the complicated mechanisms involved in the different physical processes of this material, its dielectric, electrical and magnetic behaviors are still not understood completely. In this paper we have studied the behavior of its bulk permittivity through impedance spectroscopy analysis, dielectric relaxation phenomena near the ferroelectric phase transition and detailed magnetic behavior at low temperature.

2. Experimental details

The polycrystalline sample of $Pb(Fe_{1/2}Nb_{1/2})O_3$ was prepared with starting materials; PbO, Fe_2O_3 and Nb_2O_5 (M/s Loba Chemicals, India). The physical mixture of these oxides in the required stoichiometry with 3% excess PbO (to compensate for lead loss) were mixed and homogenized in an agate mortar under dry conditions for 1 h followed by 2 h in wet medium. The physical mixture so obtained was calcined at 900 °C in air atmosphere for 6 h in a platinum crucible. The room temperature x-ray diffraction (XRD) pattern of the calcined powder was recorded for a wide range of Bragg angles 2θ ($20° \leqslant 2\theta \leqslant 80°$) using an x-ray diffractometer (Rigaku, Miniflex, Japan) for confirmation of the compound formation and preliminary structural analysis. The calcined powder was cold pressed into small cylindrical pellets (10 mm in diameter and 1–2 mm thickness) under an isostatic pressure of 5×10^6 N m^{-2} with polyvinyl alcohol (PVA) as the binder. The pellets were sintered at 900 °C for 6 h in air atmosphere. The sintered pellets were then polished to make their flat faces smooth and parallel and subsequently electroded with high purity silver paste prior to dielectric, impedance and polarization measurements. Dielectric and impedance data were measured using a computer-controlled impedance analyzer (HIOKI LCR Hi TESTER, Model 3532) in conjunction with a laboratory-made sample holder in a frequency range of 100 Hz to 1 MHz at different temperatures (28–350 °C). The P–E hysteresis loop of PFN was obtained on the poled sample using a precision work station (M/s Radiant Technologies. Inc.) The magnetic measurements were carried out in a 14 T PPMS-VSM of Quantum Design in a temperature range of 2–300 K.

3. Results and discussion

3.1. Structure and microstructure

Figure 1 shows the x-ray diffraction (XRD) pattern of the prepared polycrystalline $Pb(Fe_{1/2}Nb_{1/2})O_3$ sample recorded at room temperature. The diffraction pattern of the sample comprises of sharp single peaks of varying intensity. All the XRD peaks were indexed using a standard computer program

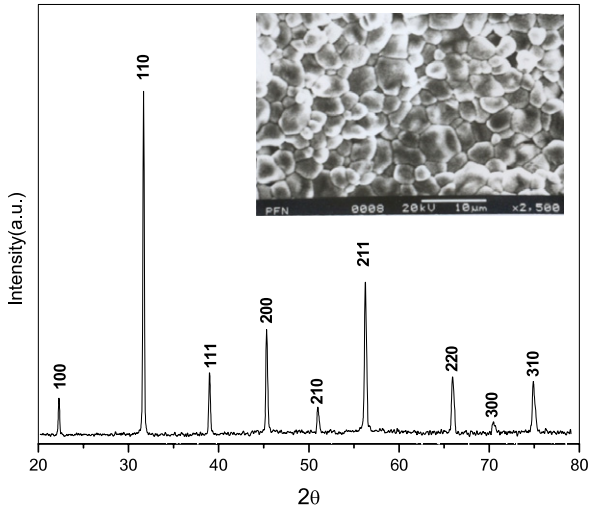

Figure 1. Room temperature XRD pattern of $Pb(Fe_{1/2}Nb_{1/2})O_3$ with SEM micrograph (inset).

POWDMULT[5]. A preliminary structural analysis suggests rhombohedral unit cell structure for the material. The least-squares refined unit cell parameters are $a = 4.0168(13)$ Å and $\alpha = 89.87°$ (the number in parentheses is the estimated standard deviation).

The SEM micrograph of the sintered pellet is shown in the inset of figure 1. The micrograph reveals a uniform distribution of grains of varying size and shape with well-defined boundaries.

3.2. Electrical properties

3.2.1. Impedance spectroscopy and dielectric properties. Impedance spectroscopy is a convenient tool to characterize the different electrically active regions in a material. It permits an unambiguous separation of the electrical response attributed to the grains (bulk) and grain boundaries in a polycrystalline sample in view of their different relaxation times [33–36]. To extract meaningful information from the impedance spectroscopy data, it is essential to model experimental data using the proper equivalent electrical circuit. In an ideal case both grain and grain boundary behavior are assumed to follow a Debye-like behavior and show two semicircular arcs in the plot of the imaginary (Z'') versus real (Z') part of the complex impedance (Z^*) (Nyquist plot). This is evident from the equation for impedance of a simple RC circuit in parallel (parallel resistance and capacitance), i.e.

$$Z^* = Z' - \mathrm{j}Z'' = \left(\frac{1}{R} + \mathrm{j}\omega C\right)^{-1}$$

where

$$Z' = \frac{R}{1 + (\omega RC)^2}, \qquad Z'' = R\left(\frac{\omega RC}{1 + (\omega RC)^2}\right)$$

and ω is the angular frequency.

[5] POWDMULT: an interactive powder diffraction data interpretation and indexing program version 2.1, E. WU School of Physical Sciences, Flinders University of South Australia, Bradford Park, SA 5042, Australia.

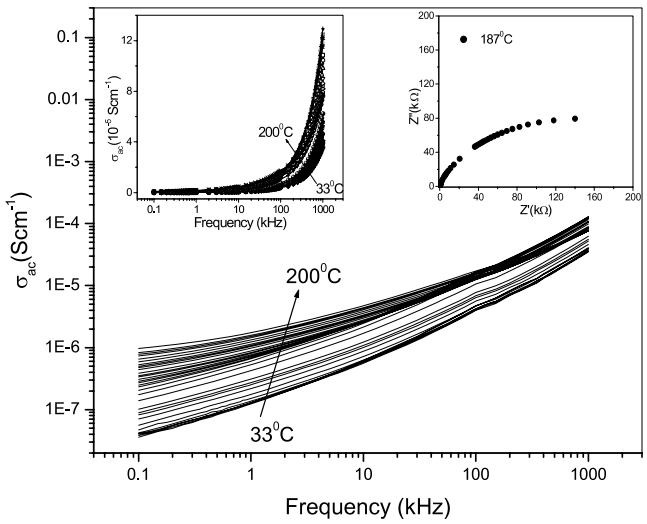

Figure 2. Variation of ac conductivity (σ_{ac}) with frequency in log–log scale and linear–log scale (top left inset) at different temperatures. A representative Nyquist plot at 187 °C is shown in the top right inset.

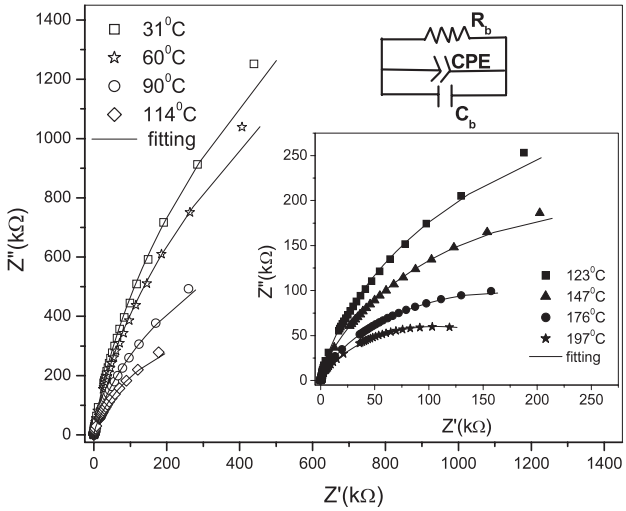

Figure 3. Nyquist plots at some selected temperatures with scattered points showing the experimental data and the solid curves showing the fitting data, according to the proposed circuit model (inset).

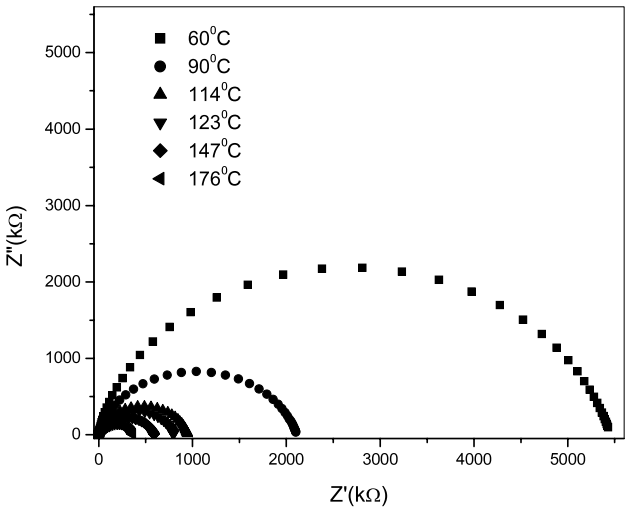

Figure 4. Nyquist plots at some selected temperatures from the simulated data of the fitting curves.

The assignment of the two semicircular arcs to electrical response due to grain interior and grain boundary can be expressed as an equivalent electrical circuit built up by cascading of two parallel resistances and capacitances (RC circuits) connected in series, each being responsible for a semicircle in the experimental electrical response and appear to be consistent with the 'brick-layer model' for a polycrystalline material [33–35]. However, in practice, instead of an ideal Debye-like response, the semicircular arcs obtained are depressed with their centers below the real axis. Generally, to represent the departures from Debye-like ideality a constant phase element, CPE, is included with the parallel RC element [33–35]. The CPEs describe the 'power law' dependence of the impedance components on frequency.

To select a proper equivalent circuit for investigating the electrical response in the temperature range below 200 °C, we have plotted the ac conductivity (σ_{ac}) versus frequency at different temperatures both in log–log scale (figure 2) and linear–log scale (top left inset of figure 2) along with a representative Nyquist plot at 187 °C (top right inset of figure 2). The Nyquist plot at 187 °C tends to be a depressed semicircle (though not complete in the observed frequency window) confirming departure from Debye-like behavior. Further, there is no tendency of a second semicircle below 200 °C, indicating negligible grain boundary contribution in this temperature range.

The conductivity spectra at different temperatures (33–200 °C) show a low frequency plateau region followed by a high frequency dispersion, implying Jonscher's universal power law [37]. Also, the absence of any humps in the conductivity spectra (top left inset of figure 2) excludes any barrier effect in this temperature range.

On the basis of the above discussion, a CPE element has been added with the RC element to explain the bulk behavior of this sample below 200 °C. CPE has impedance, given by $Z_{CPE} = [A_0(j\omega)^n]^{-1}$, where $A_0 = A/\cos(n\pi/2)$ and $j = \sqrt{-1}$. A and n are frequency-independent parameters which usually depend on temperature [38, 39]. As n represents the gradient of the linear dispersion region of conductivity spectra, it is the power law exponent in Jonscher's power law. The value of n lies between 0 and 1 ($n = 1$ for an ideal capacitor and $n = 0$ for ideal resistor). Hence, an equivalent circuit has been modeled as shown in figure 3 (top inset) to analyze the electrical process near the ferroelectric–paraelectric phase transition. The fitting curves (according to the proposed circuit) on the Nyquist plots at some selected temperatures (below 200 °C) are shown in figure 3. The discrete points represent experimental data, while solid curves represent the overall fitting using commercially available software [40]. From the figure it is obvious that a good agreement is achieved between the observed and fitting data.

Figure 4 shows the simulated data plot of the fitting curves at some selected temperatures, again indicating negligible intergranular activities within the sample in this range of temperatures.

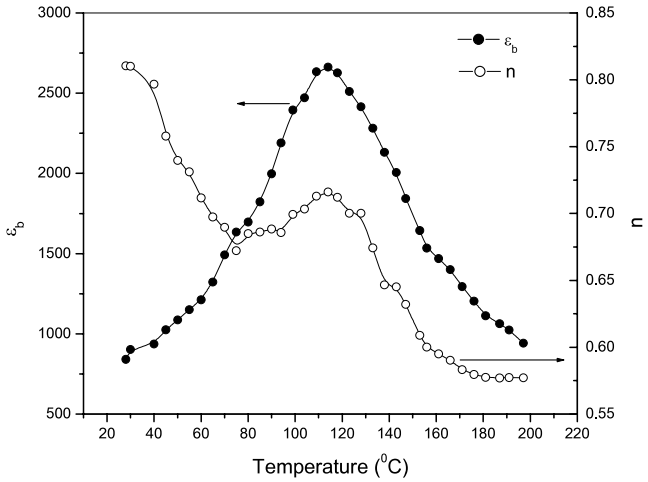

Figure 5. Variation of the bulk permittivity (ε_b) and power law exponent n with temperature.

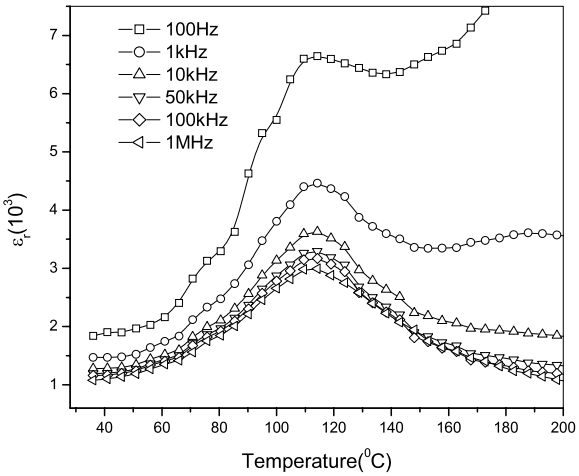

Figure 6. Variation of relative permittivity ε_r with temperature at different frequencies.

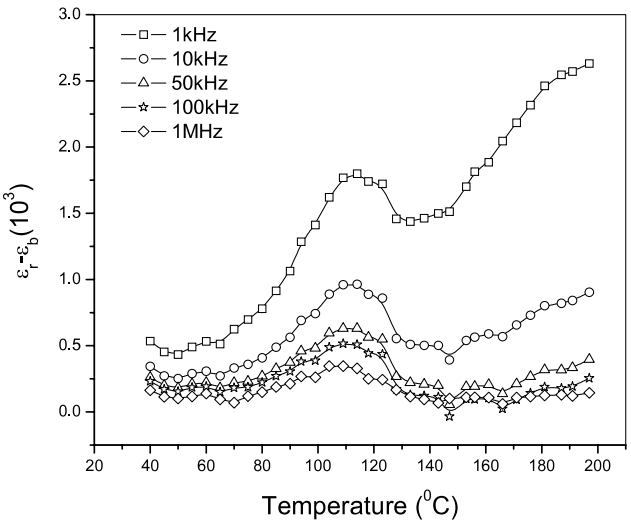

Figure 7. Variation of ε_r–ε_b with temperature at different frequencies.

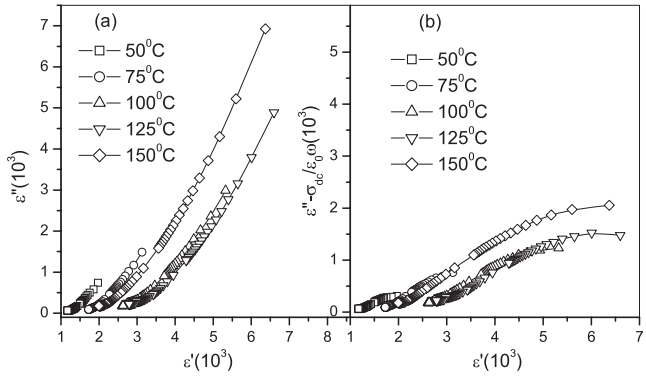

Figure 8. (a) Variation of (ε'') with (ε') and (b) variation of (ε''–$\sigma_{dc}/\varepsilon_0\omega$) with ($\varepsilon'$) at different temperatures.

The values of bulk resistance (R_b), bulk capacitance (C_b) and n were obtained from the fitting data. Using C_b/C_0 (C_0 is the vacuum capacitance of the cell without the sample), the values of bulk permittivity ε_b were calculated at different temperatures. In figure 5 the values of ε_b and n have been plotted with respect to temperature. The value of bulk permittivity gradually increases with increasing temperature (room temperature onwards) and attains a peak value at 114 °C, and then it decreases continuously. The value of n first decreases with temperature and attains a minimum value at 75 °C beyond which its value increases slowly, showing a broad peak at 114 °C. For comparison the variation of relative permittivity (ε_r) versus temperature at different frequencies is drawn (figure 6).

All the graphs show a diffused peak at the same temperature (i.e. 114 °C), which corresponds to the ferroelectric to paraelectric phase transition that agrees well with the earlier report by Bokov *et al* [2]. Also, strong low frequency dispersion is observed near the transition temperature. The temperature dependence of the bulk permittivity along with its peak at the transition temperature confirms the reliability of our proposed equivalent circuit and the corresponding data fitting.

In order to find the contribution of charge carriers to the value of permittivity, we calculated (ε_r–ε_b). The variation of (ε_r–ε_b) with temperature (figure 7) also shows a broad peak near 114 °C, and the peak value falls considerably on increasing frequency.

The charge carrier contribution to the dielectric response is evident from the nature of the Cole–Cole plot (figure 8(a)) (i.e. the graph plotted between real (ε') and imaginary (ε'') parts of the permittivity). The dc conductivity (σ_{dc}) contributes, in the frequency domain, to the imaginary part of the complex dielectric permittivity as an additional function $\sigma_{dc}/\varepsilon_0\omega$, where ε_0 and ω are the permittivity of free space and angular frequency, respectively. Subtracting $\sigma_{dc}/\varepsilon_0\omega$ from ε'', and then plotting it with respect to ε' (figure 8(b)), shows a tendency to form a depressed semicircle.

Figure 9 shows the variation of the imaginary part of permittivity (ε'') as a function of frequency (solid dots) at different temperatures in the vicinity of the ferroelectric–paraelectric transition. A strong increasing trend at low

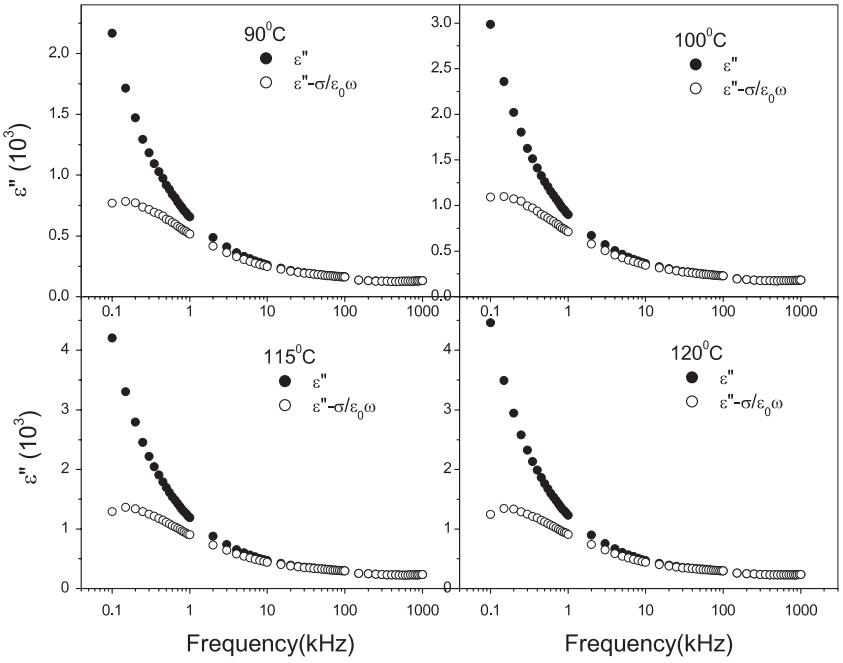

Figure 9. Variation of the imaginary part of permittivity (ε'') (solid dots) and ($\varepsilon'' - \sigma_{dc}/\varepsilon_0\omega$) (open dots) with frequency at different temperatures.

frequencies ($\leqslant$10 kHz) is an indication of the preponderance of dc conductivity.

One possible way of treating such data is to subtract the $\sigma_{dc}/\varepsilon_0\omega$ contribution from the measured value of ε''. Then the remaining part of ε'' (i.e. $\varepsilon'' - \sigma_{dc}/\varepsilon_0\omega$) is plotted (open dots) to characterize the dielectric relaxation. These curves show a peak at 150 Hz at each temperature. However, this peak disappears above 135 °C and also this peak could not be observed at lower temperatures.

3.2.2. Conductivity and polarization studies. Figure 10 shows the variation of ac conductivity (σ_{ac}) at different frequencies as well as dc conductivity (σ_{dc}) with the inverse of absolute temperature. The dc conductivity is calculated from the bulk resistance R_b, using the formula $\sigma_{dc} = \frac{l}{R_b A}$, where l is the thickness of the sample and A is the area of the electrode deposited on the sample.

All the conductivity graphs show an anomaly at the transition temperature. The anomaly is more prominent for higher frequencies. The dc conductivity increases with the rise in temperature and the nature of the variation appears to be of Arrhenius type (i.e. $\sigma = \sigma_0 e^{E_a/kT}$) below 114 °C and again above 120 °C with a small nonlinearity near the ferroelectric transition. Here E_a is the activation energy and k is Boltzmann's constant. The activation energy evaluated using this relation works out to be 0.34 eV and 0.37 eV below and above the ferroelectric transition, respectively. The variation of electric polarization (P) with applied electric field (E) of the poled sample at room temperature is shown in figure 11. The well-developed hysteresis loop shows a tendency for saturation near an applied field of 10 kV cm^{-1}, confirming the ferroelectric order in the PFN sample at room temperature.

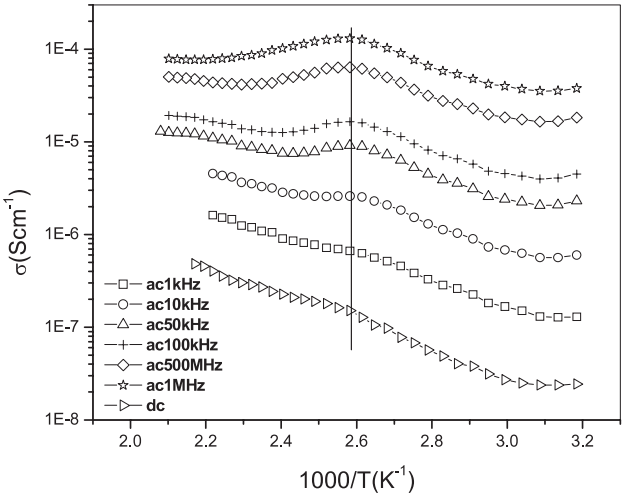

Figure 10. Variation of ac conductivity at different frequencies and dc conductivity with the inverse of absolute temperature.

The $2P_r$ (remnant polarization) value was found to be 5.62 μC cm^{-2} at a maximum applied field of 12 kV cm^{-1}.

3.2.3. Discussion. The mechanism of the diffused phase transition in PFN (without the frequency dependence of the transition temperature) has been explained by several propositions from several authors. In the present study we observed that the bulk permittivity shows the same diffuse pattern at the transition temperature. Moreover, the permittivity pattern due to charge carrier contributions alone also follows a broad anomaly pattern near the transition temperature. It is well established that in PFN there exists a disorder at the B-site and some amount of Fe^{+2} exists along

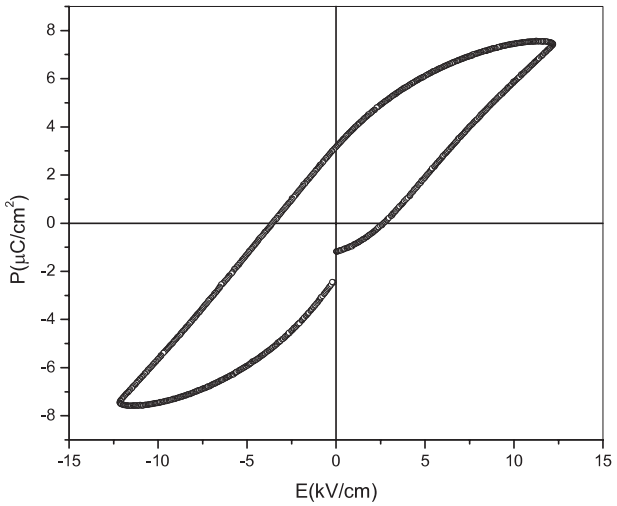

Figure 11. *P–E* loop of the poled sample at room temperature.

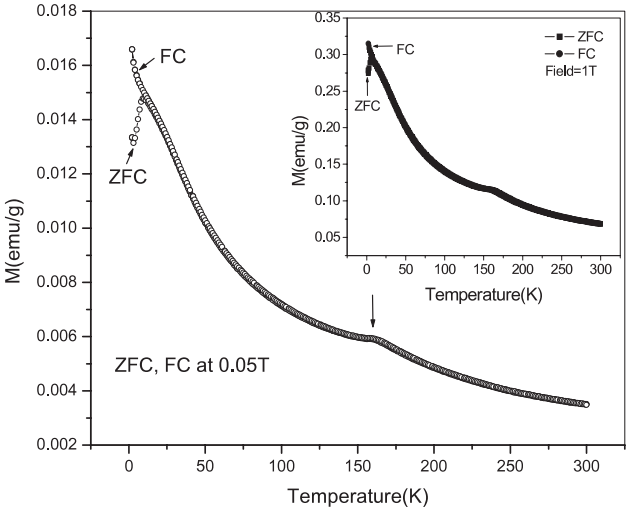

Figure 12. *M–T* curve in ZFC and FC modes at 0.05 T. *M–T* curve in ZFC and FC modes at 1 T is shown in the inset.

with Fe^{+3} ions at this site. The coexistence of Fe^{+2} and Fe^{+3} ions on equivalent crystallographic sites generally gives rise to an electron-hopping type of conduction mechanism in this material. This is evident from the value of activation energy calculated here from the dc conductivity versus temperature graph (figure 10). Therefore, a broad anomaly in the permittivity pattern due to the charge carrier contribution near the transition temperature implies that the hopping polarons influence and contribute to the diffused nature of the phase transition. Unlike that of other ferroelectric materials, the variation of power law exponent with temperature here shows a peculiar nature (figure 5). This may be due to the fluctuation in the distribution of polar microdomains, change in the degree of disorderness in the vicinity of the phase transition or the interaction of hopping polarons with the polarization within the domain. The coupling of charge carriers with the ferroelectric domains is further shown by the anomaly observed in the conductivity pattern at the transition temperature (figure 10). The peak observed in the imaginary part of the permittivity after extracting the conductivity contribution (figure 9) at such a low frequency (150 Hz) is a remarkable observation not reported before in PFN. Generally this low frequency relaxation carries an impression that it is an effect of the bad contact between the silver electrode and surface of the ceramics. If so, this should be manifested in the impedance spectra (Nyquist plot) as a low frequency spike, or a tail and a hump in the conductivity spectra. But both these features are absent, even at higher temperatures. Moreover, when electrode–PFN ceramic influences the macroscopic properties of the system, it gives rise to a very large value of permittivity [41], which is not the case here. Though further low frequency measurements are required to rule out the electrode effect completely, an otherwise tentative explanation may be given as follows.

In ferroelectric materials the relaxation observed in the mid-frequency range is often attributed to the superposition of Debye-type relaxation processes of individual domain wall segments. The relaxation frequency of domain wall vibration depends upon the domain size. Therefore, there are divergent reports on the domain wall relaxation frequency starting from very low frequency [42] to very high frequency [10] in PFN. As proposed by Park [42], we also suggest that such a low frequency relaxation may be related to irreversible motion 'creep' of domain walls. The observation of this relaxation frequency up to 135 °C, shows that polar microdomains persist up to some temperature above the transition temperature, giving the diffused nature of the phase transition. At lower temperatures the absence of this relaxation frequency may be due to the fact that domain walls become stiffer, and as a result the relaxation is suppressed.

3.3. Magnetic properties

Figure 12 shows interesting magnetic behavior of the $Pb(Fe_{1/2}Nb_{1/2})O_3$ ceramic sample.

Magnetization (M) in both zero-field-cooled (ZFC) and field-cooled (FC) modes measured at 0.05 and 1 T (inset) magnetic field, increases gradually with the decrease in temperature below 300 K. Around 158 K a kink is observed at both magnetic fields without any observable shift in the temperature. Further, there is no bifurcation in ZFC and FC magnetization modes around this kink, indicating a thermodynamic transition. The kink at 158 K, close to the earlier reported value (155 K) by Maryanowska *et al* [17], can be assigned to the antiferromagnetic Néel temperature. It may be noted that an antiferromagnetic transition around 150 K was inferred from the earlier studies on the $Pb(Fe_{1/2}Nb_{1/2})O_3$ single crystal [18]. However, unlike that of typical antiferromagnetic nature, the magnetization again increases continuously below this kink temperature, showing the existence of weak ferromagnetism. A similar increase in magnetization below the antiferromagnetic transition was also observed in the PFN single crystal which was attributed to weak ferromagnetism from the Mössbauer study, indicating that it is not an artifact arising from the polycrystalline nature of our sample. Recently Majumdar *et al* [13] and Blinc *et al* [22] have separately reported that weak

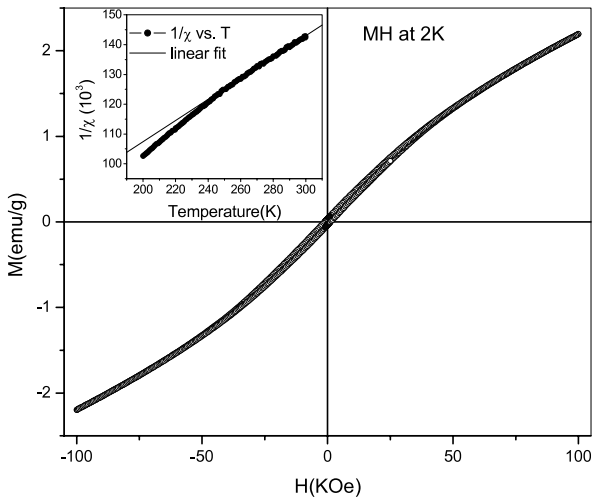

Figure 13. M–H curve at 2 K. Variation of reciprocal of magnetic susceptibility $(1/\chi)$ with temperature (200–300 K) is shown in the inset.

ferromagnetism in PFN exists even up to 300 K. The effect of weak ferromagnetism at low temperature is evident from the nonlinearity in the M–H hysteresis loop with a small opening in the loop (figure 13). The inset of figure 13 shows the variation of the reciprocal of magnetic susceptibility $(1/\chi)$ with temperature which appears to be linear above 250 K, indicating a paramagnetic phase. Thus PFN undergoes an antiferromagnetic transition followed by onset of weak ferromagnetism. It has been established by Goossens *et al* [43] that the magnetic order in perovskites can show both antiferro- and ferromagnetic components.

Another significant feature observed in figure 12 is the magnetic anomaly at low temperature when ZFC magnetization shows a peak and bifurcates from the FC magnetization. This peak in ZFC magnetization is at 9 K for 0.05 T measurement field and shifts to around 6 K when measured at a field of 1 T. It may be noted that Watanabe *et al* [16] observed a similar anomaly below 9 K and attributed it to weak ferromagnetic ordering due to the magnetoelectric effect. However, in the present sample, the bifurcation in the ZFC and FC magnetization accompanied by the shift in the ZFC peak to lower temperature with the increase in field is a thermomagnetic history-dependent feature that indicates the presence of a metastable magnetic state at low temperature. [44, 45]. Though this behavior at low temperature was reported by Falqui *et al* [46] in the PFN single crystal, the observation of such a behavior on polycrystalline PFN is reported for the first time in the present study. This is significant since in another study on the single crystal of PFN, though a weak ferromagnetism was inferred from a steep increase in magnetization below the antiferromagnetic transition, no such thermomagnetic history-dependent behavior was observed down to 4.2 K [18]. Moreover, this anomaly in the present polycrystalline sample is rather sharp even compared to the single-crystal data [46]. It may be noted that this type of metastable magnetic state is observed in the systems when ferromagnetic interactions are introduced randomly in a predominantly antiferromagnetic matrix. It is shown that, in PFN, the Fe ion prefers the Fe^{3+} high spin state but distributions of Nb and Fe are random at the B-site [19]. Therefore, some of the superexchange interactions may give rise to the observed weak ferromagnetism and a random distribution of ferromagnetic interactions in the present system. Thus it may be concluded that the distribution of Nb and Fe is actually random in our sample, which also has a significant effect on its dielectric properties. Nevertheless, this noteworthy low temperature feature in PFN needs to be investigated in detail to ascertain its nature and origin and also its relation to the magneto-electric coupling in this system.

4. Conclusion

The polycrystalline $Pb(Fe_{1/2}Nb_{1/2})O_3$ sample, prepared by a high temperature solid-state reaction technique. Preliminary structural analysis shows the formation of the material in a rhombohedral structure. The impedance data were analyzed according to an equivalent circuit selected on the basis of conductivity spectra and Nyquist plot. From the fitting data the bulk permittivity was extracted. The variation of bulk permittivity with temperature was compared with the temperature dependence of relative permittivity measured at constant frequencies. A good agreement in terms of the transition temperature between the two was observed. The power law exponent also shows a peak at the ferroelectric transition. A slow dynamics relaxation phenomenon is observed at and around the ferroelectric transition temperature. A room temperature P–E loop establishes the ferroelectric ordering in the sample. This PFN system shows an antiferromagnetic transition at 158 K. Just below the antiferromagnetic transition, the unusual increase in magnetization is attributed to the onset of a weak ferromagnetism. The nonlinear behavior of magnetization as a function of a field with a finite opening in the M–H loop, at 2 K, gives further evidence of ferromagnetism. Significantly, pronounced field-dependent thermomagnetic irreversibility below 9 K indicates a metastable magnetic state, indicating a random distribution of B-site cations in the system.

Acknowledgments

The authors acknowledge DST, Government of India for funding the VSM. One of the authors (RKM) expresses gratitude to the Government of Orissa and the principal of his parent college V N College, Jajpur Road, Orissa, India, for the grant of study leave to carry out this research work.

References

[1] Smolenskii G A, Agranovskya A I, Popov S N and Isupov V A 1958 *Sov. Phys.—Tech. Phys.* **3** 1981
[2] Bokov V A, Myl'nikova I E and Smolenskii G A 1962 *Sov. Phys.—JETP* **15** 447
[3] Yasuda N and Ueda Y 1989 *J. Phys.: Condens. Matter* **l** 497
[4] Fundora A, Azquez A V, Portelles J, Calderon F and Siqueiros J M 1998 *J. Non-Cryst. Solids* **235** 567
[5] Ananta S and Thomas N W 1999 *J. Eur. Ceram. Soc.* **19** 1873

[6] Ivanov S A, Tellgren R, Rundlof H, Thomas N W and Ananta S 2000 *J. Phys.: Condens. Matter* **12** 2393
[7] Wang Y X, Zhong W L, Wang C L and Zhang P L 2001 *Phys. Lett.* A **288** 45
[8] Bhat V V, Umarji A M, Shenoy V B and Waghmare U V 2005 *Phys. Rev.* B **72** 014104
[9] Raymond O, Front R, Saurez-Almodovar N, Portelles J and Siqueiros J M 2005 *J. Appl. Phys.* **97** 084107
[10] Raymond O, Front R, Portelles J, Saurez-Almodovar N and Siqueiros J M 2006 *J. Appl. Phys.* **99** 124101
[11] Varshney D, Choudhary R N P and Katiyar R S 2006 *Appl. Phys. Lett.* **89** 172901
[12] Yan L, Li J, Suchicital C and Viehland D 2006 *Appl. Phys. Lett.* **89** 132913
[13] Majumdar S B, Bhattacharya S, Katiyar R S, Manivannan A, Dutta P and Seehra M S 2006 *J. Appl. Phys.* **99** 024108
[14] Astrov D N, Al'shin B I, Zorin R V and Drobyshev L A 1968 *Zh. Eksp. Teor. Fiz.* **55** 2122
[15] Pietrzak J, Maryanowska A and Leciejewicz J 1981 *Phys. Status Solidi* a **65** K79
[16] Watanabe T and Kohn K 1989 *Phase Transit.* **15** 57
[17] Maryanowska A and Pietrzak J 1994 *Ferroelectrics* **162** 81
[18] Yang Y, Liu J M, Huang H B, Zou W Q, Bao P and Liu Z G 2004 *Phys. Rev.* B **70** 132101
[19] Liu J M, Li Q C, Gao X S, Yang Y, Zhou X H, Chen X Y and Liu Z G 2002 *Phys. Rev.* B **66** 054416
[20] Bhat V V, Ramanujachary K V, Lofland S E and Umarji A M 2004 *J. Magn. Magn. Mater.* **280** 221
[21] Alvarez G, Font R, Portelles J, Valenzuela R and Zamorano R 2006 *Physica* B **384** 322
[22] Blinc R, Cevc P, Zorko A, Holc J, Kosec M, Trontelj Z, Pirnat J, Dalal N, Ramachandran V and Krzystek J 2007 *J. Appl. Phys.* **101** 033901
[23] Varshney D, Choudhary R N P and Katiyar R S 2007 *Appl. Phys.* A **89** 793
[24] Smolenskii G A and Bokov V A 1964 *J. Appl. Phys.* **35** 915
[25] Hill N A 2000 *J. Phys. Chem.* B **104** 6694
[26] Hill N A and Filippetti A 2002 *J. Magn. Magn. Mater.* **242** 976
[27] Khomskii D I 2006 *J. Magn. Magn. Mater.* **306** 1
[28] Spaldin N A and Fiebig M 2005 *Science* **309** 391
[29] Eerenstein W, Mathur N D and Scott J F 2006 *Nature* **442** 759
[30] Bokov A A, Shpak L A and Rayevsky I P 1993 *J. Phys. Chem. Solids* **54** 491498
[31] Chen I W 2000 *J. Phys. Chem. Solids* **61** 197
[32] Lampis N, Franchini C, Satta G, Geddo-Lehmann A and Massidda S 2004 *Phys. Rev.* B **69** 064412
[33] MacDonald J R 1987 *Impedance Spectroscopy Emphasizing Solid Materials and System* (New York: Wiley)
[34] Abram E J, Sinclair D C and West A R 2003 *J. Electroceram.* **10** 165
[35] West A R, Sinclair D C and Hirose N 1997 *J. Electroceram.* **1** 65
[36] Gerhardt R 1994 *J. Phys. Chem. Solids* **55** 1491
[37] Jonscher A K 1977 *Nature* **267** 673
[38] Jorcin J B, Orazem M E, Pebere N and Tribollet B 2006 *Electrochim. Acta* **51** 1473
[39] Macdonald J R 1984 *Solid State Ion.* **13** 147
[40] Yeum B 2001 ZSimpWin *Electrochemical Impedance Spectroscopy Data Analysis software*
[41] Wojcik K, Zieleniiec K and Milata M 2003 *Ferroelectrics* **289** 107
[42] Park Y 2000 *Solid State Commun.* **113** 379
[43] Goossens D J, Robinson R A and Telling M T F 2004 *Physica* B **352** 105
[44] Binder K and Young A P 1986 *Rev. Mod. Phys.* **58** 801
[45] Mydosh J A 1993 *Spin Glasses: an Experimental Introduction* (London: Taylor and Francis)
[46] Falqui A, Lampis N, Geddo-Lehmann A and Pinna G 2005 *J. Phys. Chem.* B **109** 22967